NRC Research Press

ARTICLE

Induced energy polarization of the vacuum and the rotational curves of spiral galaxies

A. Raymond Penner

Abstract: The theory of an induced energy polarized vacuum is used to determine the rotational curves for modeled galaxies whose baryonic mass distribution parameters are the median values of three classes of spiral galaxies. From the theoretical curves it is found that the bulge contribution plays a dominant role in determining the behavior of the rotational curves in the inner regions (i.e., within three disc scale lengths). For the outer regions the theoretical rotational curves for all the galaxies behave similarly as they slowly fall to the asymptotic value as determined by the baryonic Tully–Fisher relationship. Overall it is found that rotational curves generated by the induced energy polarized vacuum theory can readily produce observed features in the rotational curves of spiral galaxies.

PACS Nos.: 90.95.30.–k.

Résumé : Nous utilisons la théorie d'un vide polarisé à énergie induite pour déterminer les courbes de (la vitesse de) rotation de galaxies modèles dont les paramètres de distribution de masse ont la valeur médiane de trois classes de galaxies spirales. À partir des courbes théoriques, nous trouvons que la contribution du cœur galactique joue un rôle dominant dans le comportement des courbes de rotation des régions intérieures, (i.e. à l'intérieur de trois longueurs d'échelle du disque). Les courbes théoriques de rotation des régions externes pour toutes les galaxies spirales tendent asymptotiquement vers les valeurs déterminées par la masse baryonique de Tully–Fisher. De façon générale, nous trouvons que les courbes de rotation causées par un vide polarisé à énergie induite sont facilement capables de reproduire les caractéristiques des courbes de rotation des galaxies spirales. [Traduit par la Rédaction]

1. Introduction

Galactic rotation curves are the major tool used in determining the overall mass distribution in spiral galaxies. Obtaining complete central-to-outer rotation curves for galaxies is, however, a significant challenge and typically requires a combination of different observational wavelengths. Examples of such central-to-outer galactic rotational curves as provided in ref. 1 are shown in Fig. 1. These rotational curves are a subset of those given in ref. 2, specifically those curves that have the greatest range. In general, as is seen with these and other rotation curves, the rotational curves are found to either remain at relatively constant values beyond ~10 kpc or at the most to decrease very slowly. A relationship is also found between this approximately constant outer rotational velocity, v, and M, the total baryonic mass of the galaxy. This baryonic Tully–Fisher relationship (BTFR) as given in ref. 3 is

$$M = AM_{\odot}v^4 \tag{1}$$

with $A = (45 \pm 10)$ km^{-4} s^4. As is also seen in Fig. 1, the primary differences between galactic rotational curves are found in the inner regions (i.e., within 10 kpc).

The most important result related to galactic rotation curves is that the observed outer rotational velocities greatly exceed what is predicted from the stellar distributions. This is one of the major observations that has given rise to dark matter theory. In dark matter theory, the dark matter, (whatever it may be), is the dominant mass component of a galaxy and provides the required additional contribution to the galaxy's rotation curve. A simple model of the distribution of dark matter is the semi-isothermal spherical distribution [4, 5]. In this model the density profile of the dark matter is given by

$$\rho_{\rm iso}(r) = \frac{\rho_{0,\rm iso}}{1 + (r/r_{\rm s})^2} \tag{2}$$

where $\rho_{0,\rm iso}$ is the central mass density and $r_{\rm s}$ is the scale radius of the dark matter halo. For $r \gg r_{\rm s}$ this distribution behaves as r^{-2}, which leads to a flat rotation curve at large distances. The asymptotic rotation velocity for this semi-isothermal distribution is given by

$$v_{\rm asym} = \sqrt{4\pi G\rho_{0,\rm iso}r_{\rm s}^2} \tag{3}$$

A model based on numerical simulations of the formation of galaxies, known as the Navarro–Frenk–White (NFW) model [6], has the dark matter density profile behaving as

$$\rho_{\rm NFW}(r) = \frac{\rho_{0,\rm NFW}}{(r/r_{\rm s})[1 + (r/r_{\rm s})]^2} \tag{4}$$

This distribution yields an infinitely increasing density as the galactic centre is approached and for $r \gg r_{\rm s}$ behaves as r^{-3}. Instead of the rotation curve approaching a constant velocity at large radius, as with the semi-isothermal model, this profile leads to a slowly decreasing rotation curve. The semi-isothermal and NFW energy density profiles are shown in Fig. 2. For the semi-isothermal

Received 7 February 2013. Accepted 24 April 2013.

A.R. Penner. Department of Physics, Vancouver Island University, 900 Fifth Street, Nanaimo, BC V9R 5S5, Canada.
E-mail for correspondence: raymond.penner@viu.ca.

Fig. 1. Complete central-to-outer rotation curves as provided by refs. 1 and 2. (*a*) NGC 1097; (*b*) NGC 2841; (*c*) Milky Way; (*d*) NGC 5035; (*e*) NGC 4565; (*f*) NGC 1365; (*g*) NGC 224; (*h*) NGC 5907; and (*i*) NGC 3198. The rotational velocities are in kilometres per second and the distances are in kiloparsecs.

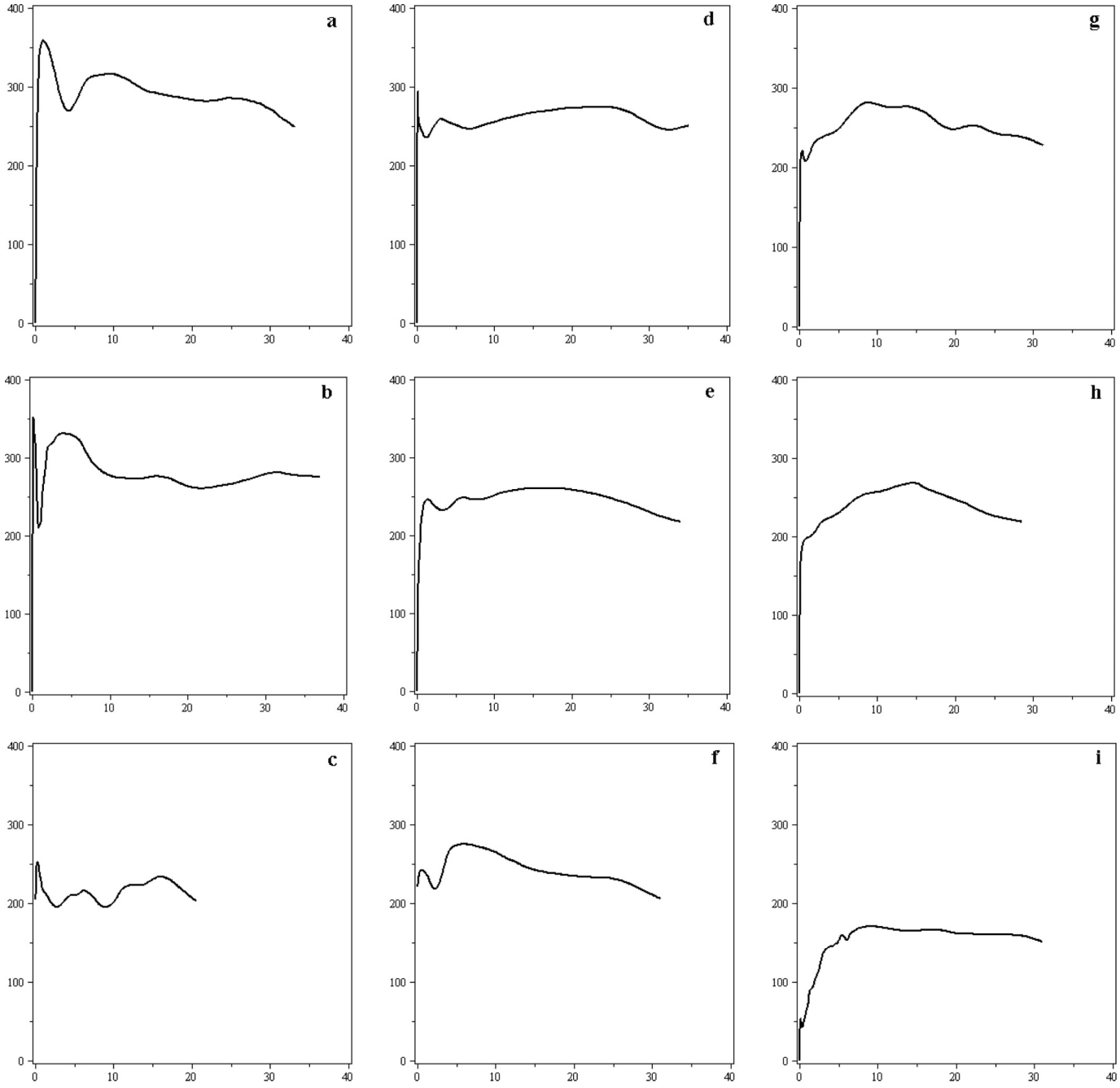

model the scale radius has been set to 5 kpc and v_{asym} has been set to 191 km/s. For the NFW model the scale radius has also been set to 5 kpc and the value of $\rho_{0,NFW}$ is set so that both distributions have the same value at 20 kpc. The scale radius for the dark matter distribution for either of these two models is not explicitly correlated to the baryonic mass distribution. Typically, the dark matter contribution to the rotation curve of a galaxy is obtained post facto by subtracting out the modeled contribution of the baryonic matter from the observed rotation curve [7, 8] or by finding a best fit for modeled baryonic and dark matter contributions [9]. In general, in dark matter theory the correlation between the dark matter distribution and the baryonic mass distribution is either weak or absent altogether. As such dark matter theory does not lead to the BTFR.

In refs. 10 and 11, the author presented an alternative to dark matter theory wherein the correlation between the baryonic mass distribution and a galaxy's rotation curve is very strong. In this theory the baryonic mass of the galaxy polarizes the vacuum with respect to energy, which results in the vacuum providing an additional contribution to the gravitational field. In some sense, for this theory it is the baryonic mass itself that generates the "dark matter". Unlike the density distributions of dark matter there is no specific distribution in the induced energy polarized vacuum theory. The specific baryonic distribution of a particular galaxy

Fig. 2. Semi-isothermal (solid line) and NFW (dashed line) dark matter density profiles with the scale radius set to 5 kpc.

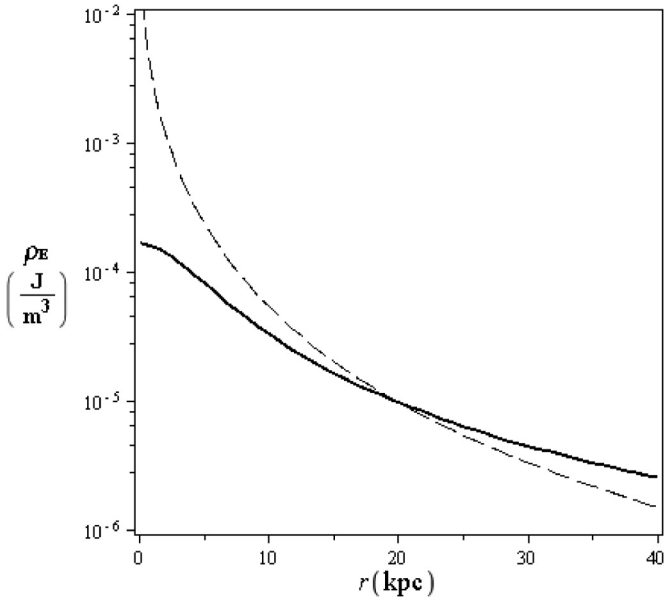

will determine the energy density distribution of the polarized vacuum and this distribution, like spiral galaxies themselves, will generally not be isotropic. The baryonic mass of a galaxy combined with the polarized vacuum contribution will determine the gravitational field of a given galaxy and in turn its rotation curve. This alternate theory also leads naturally to the BTFR and was used to determine the rotation curve of the Galaxy [11]. The primary goal of this paper is to show that the theory of an induced energy polarized vacuum also agrees generally with the observed behavior seen with the rotational curves of spiral galaxies.

The outline of this paper is as follows. In Sect. 2 the elements of the theory of an induced energy polarized vacuum that are required to generate galactic rotation curves will be presented. In Sect. 3 a model of the baryonic mass distribution of spiral galaxies will be provided and the mean values of galactic parameters for three different Hubble stages will be determined. Section 4 will present the simulated rotation curves for the representative galaxies of Sect. 3 and will compare their features to those seen in the observed rotation curves of Fig. 1.

2. Energy polarization of the vacuum

In refs. 10 and 11, a semiclassical model of how the vacuum becomes energy polarized in a gravitational field is presented. A brief summary will be presented in this section. It is hypothesized that throughout the cosmos entities of both net positive and net negative energy continually come into and out of existence with a maximum lifetime, τ, as given by the Heisenberg uncertainty principle. In the presence of a gravitational field each entity will shift during its lifetime and subsequently each entity will be equivalent to an energy dipole. In refs. 10 and 11, a model of the effect that interactions between the entities has on their lifetimes and thereby on the amount that they shift results in the following dependence that $\boldsymbol{P}_E$, the induced energy dipole moment density, has on $\boldsymbol{g}$, the total gravitational field,

$$\boldsymbol{P}_E = \frac{c^2}{4\pi G} g_0 \left[\frac{3}{2}\left(1 - \frac{e^{-\gamma(g/g_0)}}{\gamma}\right)\right]\hat{\boldsymbol{g}} \tag{5}$$

where

$$\gamma = \frac{\sqrt{\pi}}{2}\frac{\mathrm{erf}\left(\sqrt{\gamma(g/g_0)}\right)}{\sqrt{\gamma(g/g_0)}} \tag{6}$$

The value of the single parameter g_0 in (5) and (6) is given by

$$g_0 = \frac{3}{2GA} \tag{7}$$

where A is the coefficient of the BTFR. For the value of A given for (1) this leads to

$$g_0 = (1.0 \pm 0.2) \times 10^{-10}\ \mathrm{m\ s^{-2}} \tag{8}$$

Given the preceding energy dipole moment energy density the resulting energy density of the vacuum, ρ_E, surrounding a given gravitational field source is given by

$$\rho_E = -\nabla \cdot \boldsymbol{P}_E \tag{9}$$

The contribution to the gravitational potential, $\Phi_V(r)$, due to the energy polarized vacuum is in turn given by

$$\Phi_V = \frac{G}{c^2}\int_{V'} \frac{\rho_E dV'}{r - r'} \tag{10}$$

and the total gravitational potential, Φ, surrounding a galaxy is therefore

$$\Phi = \Phi_B + \Phi_V \tag{11}$$

where Φ_B is the gravitational potential due to the baryonic mass. The total gravitational field can then be determined by

$$\boldsymbol{g} = \nabla\Phi \tag{12}$$

In the induced energy polarized vacuum theory the rotation curve of a galaxy is therefore determined solely by the baryonic mass distribution of the galaxy and the coefficient of the BTFR. Unlike dark matter models there are no free parameters that can be adjusted to obtain a best fit. The method of obtaining the rotation curve for a given galaxy is as follows. The initial estimate of the gravitational potential and the gravitational field surrounding a given galaxy is taken to be solely that due to the galaxy's baryonic mass. The value of $\boldsymbol{P}_E$ and the resulting energy density of the vacuum are then determined by (5) and (9). From the energy density distribution the gravitational potential due to the vacuum is then determined using (10) and for the next estimate the total gravitational potential is taken to be equal to the sum of the potentials due to the baryonic mass and the vacuum. This iterative process is repeated until the far field values of the total gravitational field obtained after a given iteration vary by less than 1% from the previous iteration. The rotational velocity is then found using $v = \sqrt{gr}$, where g is the total gravitational field and r is the distance from the galactic centre. In ref. 11 this was the method used to obtain the rotational curve of the Galaxy.

3. Model of the baryonic mass distribution of a galaxy

Stellar luminosity profiles for spiral galaxies are typically resolved into a spherically symmetric bulge component and an exponential disc component. One of the most widely used empirical

laws to describe the surface brightness of a galactic bulge is deVaucoulers' law, which is given by

$$I_{\mathrm{BULGE}}(r) = I_0 \exp\left[-\left(\frac{r}{r_0}\right)^{1/4}\right] \tag{13}$$

where I_0 is the central surface brightness and r_0 is a scale radius. Unfortunately the deprojected mass density is not analytically tractable for this law. However, to a good approximation the Hernquist profile, which is given by

$$\rho_{\mathrm{BULGE}}(r) = \frac{M_{\mathrm{BULGE}}}{2\pi}\frac{a}{r}\frac{1}{(r+a)^3} \tag{14}$$

with

$$a \cong \frac{r_{\mathrm{e}}}{1.82} \tag{15}$$

can be used, where M_{BULGE} is the mass of the bulge, a is a scale radius, and r_{e} is the radius that encloses half of the total bulge luminosity. The corresponding gravitational potential corresponding to the Hernquist profile is

$$\Phi_{\mathrm{BULGE}}(r) = -\frac{GM_{\mathrm{BULGE}}}{r+a} \tag{16}$$

The exponential disk luminosity profile is in turn given by

$$I_{\mathrm{DISC}}(r) = I_0 \mathrm{e}^{-r/h} \tag{17}$$

where r is the distance from the galaxy's axis, I_0 is the central surface brightness of the disc, and h is the disc scale length. The surface mass density follows the same exponential form and the resulting gravitational potential due to the disc in cylindrical coordinates is given by

$$\Phi_{\mathrm{DISC}}(r,z) = -\frac{2G}{\pi}\frac{M_{\mathrm{DISC}}}{h^2}\int_0^\infty \frac{x\exp(-x/h)K\left(\sqrt{4xr/q^2}\right)}{q}dx \tag{18}$$

where $q = [z^2 + (x+r)^2]^{1/2}$, M_{DISC} is the mass of the disc, and K is the complete elliptic integral of the first kind. The total gravitational potential due to the baryonic mass distribution of a galaxy is thereby given by

$$\Phi_{\mathrm{B}} = \Phi_{\mathrm{BULGE}} + \Phi_{\mathrm{DISC}} \tag{19}$$

Given the preceding model the following parameters will specify the baryonic mass distribution of a spiral galaxy; (*i*) the ratio of the baryonic mass in the bulge to that in the disc, or the B/D ratio; (*ii*) h, the scale length of the disc; and (*iii*) r_{e}/h, the ratio of the scale length of the bulge to the scale length of the disc.

Galaxies are typically classified according to their morphologies with the most famous classification scheme being the Hubble sequence, which divides galaxies into ellipticals, spirals, lenticulars, and irregulars. The more elaborate deVaucoulers system for classifying galaxies is a widely used extension to the Hubble sequence and in this scheme numerical values are assigned to each class of galaxy. This numerical value, labeled T and referred to as the Hubble stage, runs from +1 to +7 for spiral galaxies. For spiral galaxies, the Hubble stage is primarily correlated with the appearance of the arms, specifically how tightly wound they are. As such the correlation between the Hubble stage and the baryonic mass distribution of galaxies is not very strong. However, for the purposes of this paper, baryonic mass distributions will be determined for what can be considered as representative $T = 1$, 3, and 5 spiral galaxies. From these modeled baryonic mass distributions sample rotational curves will be generated.

In ref. 12, the following expression for the relationship between Δm, the average magnitude difference between the luminosity of the bulge (B-band) and the total luminosity of the galaxy, and the Hubble stage is provided:

$$\Delta m = 0.800 + 0.145T + 0.0284T^2 + 0.002\,67T^3 \tag{20}$$

If the approximation is made that the baryonic mass distribution traces the luminosity distribution, which implies the same mass-to-light ratio in both the bulge and the disc, (20) then leads to the following median B/D ratios for the three modeled galaxy stages.

$$T = 1 \quad \langle \mathrm{B/D} \rangle = 0.686 \tag{21a}$$

$$T = 3 \quad \langle \mathrm{B/D} \rangle = 0.311 \tag{21b}$$

$$T = 5 \quad \langle \mathrm{B/D} \rangle = 0.104 \tag{21c}$$

The scatter in the values of B/D for any particular stage is found to be very large with a wide overlap between the stages. From the relationships given in ref. 13, the relationship between the disc scale length, h, and the galaxy rotation velocity was obtained for spiral galaxies. Equating the galaxy rotation velocity to the BTFR velocity then leads to the following relationships between the median disc scale lengths and the total baryonic mass of a galaxy

$$T = 1 \quad \langle h \rangle = (3.98 \times 10^{-5}\ \mathrm{kpc})\left(\frac{M}{M_\odot}\right)^{0.454} \tag{22a}$$

$$T = 3 \quad \langle h \rangle = (1.35 \times 10^{-3}\ \mathrm{kpc})\left(\frac{M}{M_\odot}\right)^{0.320} \tag{22b}$$

$$T = 5 \quad \langle h \rangle = (2.33 \times 10^{-3}\ \mathrm{kpc})\left(\frac{M}{M_\odot}\right)^{0.301} \tag{22c}$$

As with B/D ratios, the values given by (22*a*)–(22*c*) are median values and the scatter and overlap between stages is again very large. In ref. 14, the following relationship between the median value of r_{e}/h and the Hubble stage for spiral galaxies is provided

$$\left\langle \frac{r_e}{h} \right\rangle = 0.200 - 0.013(T-5) \tag{23}$$

Equation (23) leads to

$$T = 1 \quad \left\langle \frac{r_{\mathrm{e}}}{h} \right\rangle = 0.252 \tag{24a}$$

$$T = 3 \quad \left\langle \frac{r_{\mathrm{e}}}{h} \right\rangle = 0.226 \tag{24b}$$

$$T = 5 \quad \left\langle \frac{r_{\mathrm{e}}}{h} \right\rangle = 0.200 \tag{24c}$$

As with the B/D ratios and the disc scale lengths, the scatter and overlap between stages is very large.

Table 1. The median values of B/D, h (kpc), and r_e/h for modeled galaxies of Hubble stages $T = 1$, 3, and 5.

Mass ($M_\odot$)	Parameter	$T = 1$	$T = 3$	$T = 5$
180×10^9	B/D	0.686	0.311	0.104
180×10^9	h	5.13	5.40	5.69
180×10^9	r_e/h	0.252	0.226	0.200
60×10^9	B/D	0.686	0.311	0.104
60×10^9	h	3.11	3.80	4.09
60×10^9	r_e/h	0.252	0.226	0.200
20×10^9	B/D	0.686	0.311	0.104
20×10^9	h	1.89	2.67	2.94
20×10^9	r_e/h	0.252	0.226	0.200

4. Simulated rotation curves

Theoretical rotational curves were generated for galaxies of total baryonic masses of $180 \times 10^9\ M_\odot$, $60 \times 10^9\ M_\odot$, and $20 \times 10^9\ M_\odot$ for each of the three Hubble stages, $T = 1$, 3, and 5, with parameters equal to the median parameters as determined in Sect. 3 and as listed in Table 1.

As an example of the derived rotation curves, Fig. 3 shows the resulting rotational curve and the contributions from the bulge, disc, and the induced energy polarized vacuum for the representative $T = 3$ spiral galaxy of total baryonic mass of $60 \times 10^9\ M_\odot$ with the parameters as given in Table 1. For a baryonic mass of $60 \times 10^9\ M_\odot$ the BTFR of (1) leads to an asymptotic rotational velocity of 191 km/s. This is the value that both the contribution of the induced energy polarized vacuum and the total rotational curve approaches. As seen in the figure the rotational curve initially follows that of the bulge. A dip at ~2 kpc is then followed by a broad maxima with a peak value of ~225 km/s at ~11 kpc, which corresponds to a distance of approximately three disc scale lengths. Then the rotational curve slowly falls, reaching a value of ~205 km/s at a distance of 40 kpc. The rotational curve will continue to fall beyond 40 kpc as it approaches the asymptotic rotational velocity value of 191 km/s. Figure 3 shows that the induced energy polarized vacuum is the dominant contributor to the rotational curve for $r >$ ~8 kpc.

The energy density profile of the polarized vacuum for this simulation is shown in Fig. 4. As the baryonic mass distribution is nonisotropic, so is the energy density distribution for the polarized vacuum. The energy density profile is therefore provided in Fig. 4 both in the plane of the disc and perpendicular to it. The energy density profiles drop off as r^{-2} for large r and thereby lead to a rotational curve approaching a constant value. The energy density profile along the disc and perpendicular to it merge at large r as the overall energy density distribution will become isotropic. The offset seen in the figure for $r > 30$ kpc is not a real feature but a result of the relatively low resolution in the simulation due to computational limitations of the author's PC. Comparing Fig. 4 with Fig. 2 it can be seen that while the energy density profile due to the polarized vacuum is similar in behavior to the dark matter hypothesized distributions, there are crucial differences. First, there are no parameters that are set, such as r_s and ρ_0 in (2) and (4), to arrive at the energy density distributions in Fig. 4. The distributions shown in Fig. 4 are determined by the baryonic mass distribution of the given galaxy and the physical model of the induced energy polarized vacuum. The energy density distribution surrounding a galaxy will therefore change when the galaxy's baryonic mass distribution is changed and changing the total baryonic mass of the galaxy will change the distribution such that the BTFR naturally results.

Figure 5 shows all nine simulated rotational curves for the representative galaxies whose parameters are listed in Table 1. The general behavior of the rotational curves follows the behavior discussed for Fig. 3. It is seen in Fig. 5 that while the total baryonic mass of a galaxy determines the asymptotic velocity that the outer rotational curve approaches, the general behavior of the rotational curves is relatively independent of the total baryonic mass. As has been indicated, the scatter in the parameter values listed in Table 1 is very large. As an example of the effect that the scale length has on the rotational curves, Fig. 6 shows rotational curves for galaxies that have a total baryonic mass of $60 \times 10^9\ M_\odot$ and with the B/D and r_e/h ratios as given in Table 1 but with disc scale lengths of $1/2\langle h\rangle$, $\langle h\rangle$, and $3/2\langle h\rangle$. As is seen in Fig. 6, the effect of scale length on the behavior of the rotation curves is as important as the B/D ratio. In both Figs. 5 and 6 the distance corresponding to three disc scale lengths is indicated. This position corresponds

Fig. 3. The theoretical rotation curve and the contributions from the bulge, the disc, and the polarized vacuum for a $T = 3$ modeled galaxy of mass $60 \times 10^9\ M_\odot$.

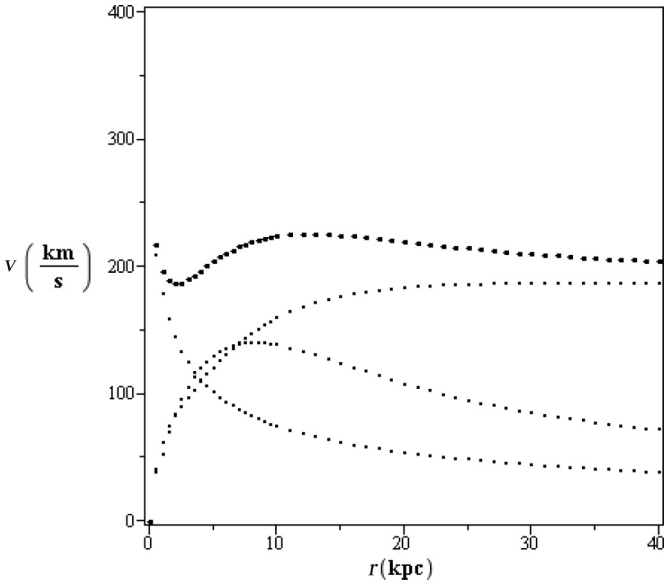

Fig. 4. Induced energy polarized vacuum density profiles both in the plane of the disc (filled-in dots) and perpendicular to it (open circles) for a $T = 3$ modeled galaxy of mass $60 \times 10^9\ M_\odot$.

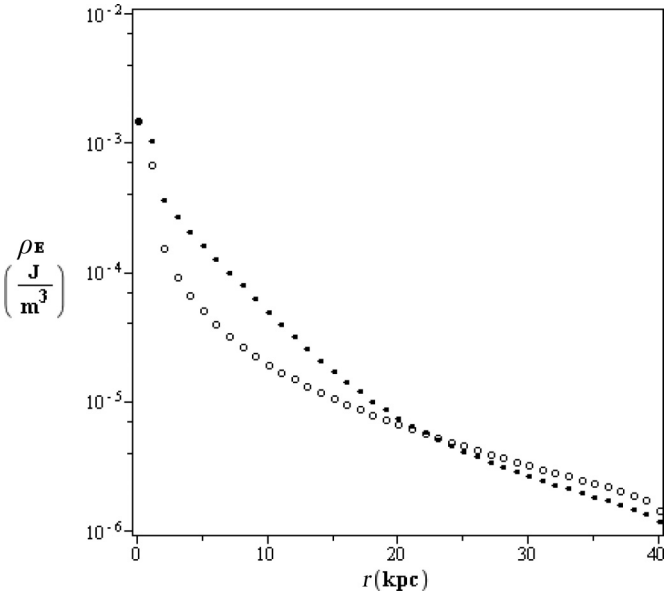

Fig. 5. Theoretical rotation curves and the contributions from the bulge, the disc, and the polarized vacuum for modeled $T = 1$, 3, and 5 galaxies of mass $20 \times 10^9\ M_\odot$, $60 \times 10^9\ M_\odot$, and $180 \times 10^9\ M_\odot$. The rotational velocities are in kilometres per second and the distances are in kiloparsecs.

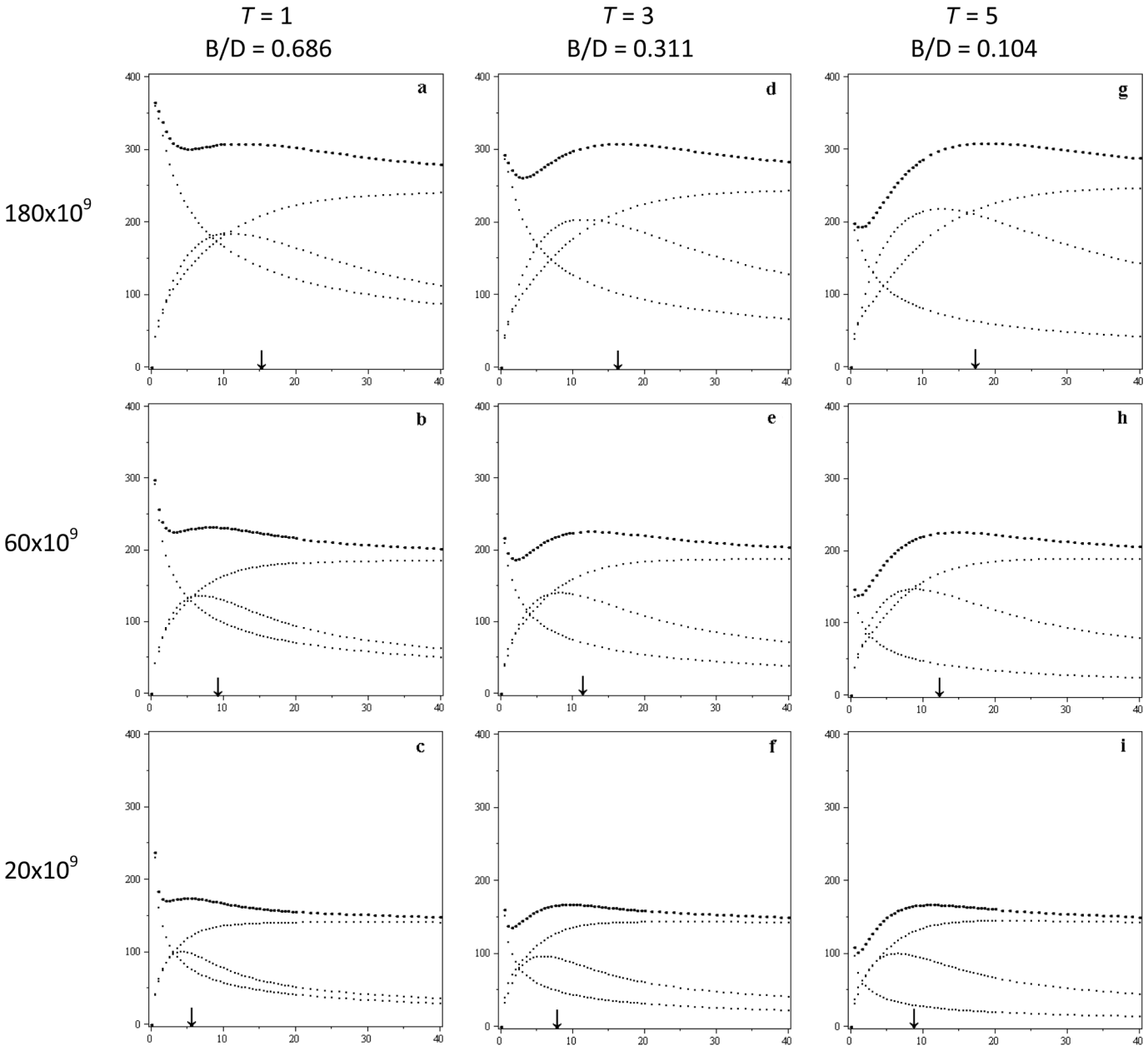

approximately to the position of the maxima as discussed previously with Fig. 3. With respect to this position there are two general conclusions that can be made with regards to the theoretical rotation curves:

1. The behavior of the inner rotation curves (i.e., $r < 3h$) is primarily determined by the baryonic mass distribution of the galaxy, with the bulge being the dominant contributor to the rotational curve in the very inner regions (i.e., $r \leq h$). The strong dependence of the inner rotational curve on the bulge contribution is very evident in Fig. 5 as one moves from the $T = 1$ galaxies with a B/D of 0.686 to $T = 5$ galaxies with a B/D = 0.104.
2. The behavior of the outer rotational curves (i.e., $r > 3h$) is very similar for all the galaxies and is primarily determined by the contribution from the induced energy polarized vacuum. Figure 5 shows that all the rotational curves slowly approach their asymptotic rotational velocity, with a drop in rotational velocity from the maxima to the asymptotic value of approximately 15%, increasing slightly for the larger mass galaxies. The asymptotic velocity itself is determined solely by the total baryonic mass of the galaxy as per the BTFR.

The observed rotational curves shown in Fig. 1 are for galaxies classified as types T = 3–5. But again, a galaxy's baryonic mass distribution is only weakly correlated with its stage; as such, the focus will be on the general behavior that is observed for the rotational curves of spiral galaxies. To assist with this the rotational curves in Fig. 1 have been arranged from Fig. 1*a* to Fig. 1*i* according to their apparent bulge contribution. Ignoring the individual dips and bumps, which are most likely due to observational uncertainties and secondary baryonic mass features, such as arms and bars, the rotational curves of Figs. 5 and 6 are in

Fig. 6. Theoretical rotation curves and the contributions from the bulge, the disc, and the polarized vacuum for modeled $T = 3$ galaxies of mass $60 \times 10^9 M_\odot$ with disc scale lengths of $1/2\langle h\rangle$, $\langle h\rangle$, and $3/2\langle h\rangle$. The rotational velocities are in kilometres per second and the distances are in kiloparsecs.

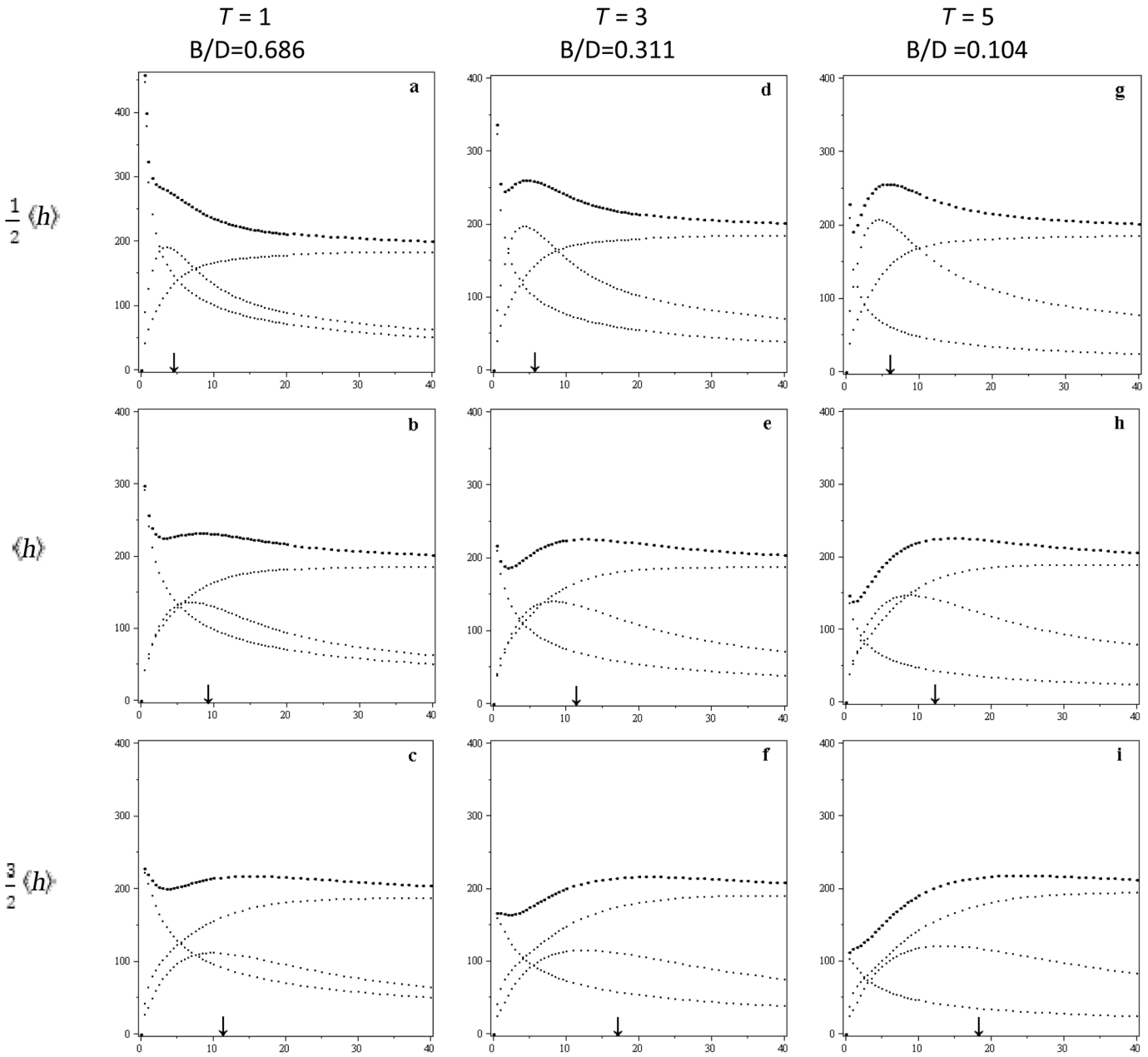

general agreement with what is observed, both in the inner and the outer regions. Great examples are provide by comparing Figs. 1*a* and 5*a*, Figs. 1*g* and 5*g*, Figs. 1*f* and 6*g*. Indeed all of the curves in Fig. 1 can by suitably matched with the theoretical curves shown in Figs. 5 and 6. Given that the theoretical rotational curves only cover a subset of the different possibilities, and considering the wide scatter in parameters that is found with galaxies, the overall agreement between the general behavior of the theoretical rotational curves and those shown in Fig. 1 is indeed very good. It is therefore concluded that rotational curves generated by the induced energy polarized vacuum theory can readily produce observed features in the rotational curves of spiral galaxies.

5. Conclusion

The theory of an induced energy polarized vacuum has been used to model the rotational curves for galaxies whose baryonic mass distribution parameters are the median values found with three classes of spiral galaxies. From the theoretical curves it is found that the bulge contribution plays a dominant role in determining the behavior of the inner curve (i.e., within three disc scale lengths). For the outer regions the theoretical rotational curves for all the galaxies behave similarly and slowly fall to the asymptotic value as determined by the BTFR. The overall behavior of the theoretical rotational curves is found to agree very well with observed rotational curves, examples of which are provided in Fig. 1.

The theory of an induced energy polarized vacuum is a marked departure from the current models for dark matter. Unlike the dark matter models, the baryonic mass of a galaxy both directly and indirectly via the induced energy polarization of the vacuum, solely determines the total gravitational field surrounding a galaxy and subsequently the galaxy's rotational curve. In addition,

unlike dark matter models, which have free parameters that are adjusted for each galaxy, the only parameter in the energy polarized vacuum model is determined experimentally by the coefficient of the BTFR.

The focus of this paper is to show that the general behavior of galactic rotational curves generated by the theory of an induced energy polarized vacuum agrees with what is actually observed. Future work will consider specific galaxies where the baryonic mass distribution can be determined with reasonable accuracy. Another area to which the author's theory of an induced energy polarized vacuum will be applied is galactic clusters. This is in fact where the idea of dark matter first originated [15]. From a model of the baryonic mass distribution of a cluster the theory will be able to determine the resulting vacuum contribution to the total gravitational field and thereby the dynamics of the cluster.

References

1. Y. Sofue, Y. Tutui, M. Honma, A. Tomita, T. Takamiya, J. Koda, and Y. Takeda. Rotation curves of spiral galaxies. Part 2. Available from: http://www.ioa.s.u-tokyo.ac.jp/~sofue/RC99/rc99.htm. 1999.
2. Y. Sofue, Y. Tutui, M. Honma, A. Tomita, T. Takamiya, J. Koda, and Y. Takeda. Astrophys. J. **523**, 136 (1999). doi:10.1086/307731.
3. S.S. McGaugh and J. Wolf. Astrophys. J. **722**, 248 (2010). doi:10.1088/0004-637X/722/1/248.
4. S.M. Kent. Astron. J. **91**, 1301 (1986). doi:10.1086/114106.
5. K.G. Begeman, A.H. Broeils, and R.H. Sanders. Mon. Not. R. Astron. Soc. **249**, 523 (1991).
6. J.F. Navarro, C.S. Frenk, and S.D.M. White. Astrophys. J. **462**, 563 (1996). doi:10.1086/177173.
7. S.A. Kassin, R.S. deJong, and B.J. Weiner. Astrophys. J. **643**, 804 (2006). doi:10.1086/502959.
8. W.J.G. deBlok and A. Bosma. Astron. Astrophys. **385**, 816 (2002). doi:10.1051/0004-6361:20020080.
9. Y. Sofue. Astrophys. J. **458**, 120 (1996). doi:10.1086/176796.
10. A.R. Penner. Can. J. Phys. **90**, 315 (2012). doi:10.1139/p2012-029.
11. A.R. Penner. Can. J. Phys. **91**, 126 (2013). doi:10.1139/cjp-2012-0300.
12. F. Simien and G. deVaucouleurs. Astrophys. J. **302**, 564 (1986). doi:10.1086/164015.
13. S. Courteau, A.A. Dutton, F.C. van den Bosch, L.A. MacArthur, A. Dekel, D.H. McIntosh, and D.A. Dale. Astrophys. J. **671**, 203 (2007). doi:10.1086/522193.
14. L.A. MacArthur and S. Courteau. Astrophys. J. **582**, 689 (2003). doi:10.1086/344506.
15. F. Zwicky. Helv. Phys. Acta, **6**, 110 (1933). doi:10.1007/s10714-008-0707-4.